01 May 2016

Strong Coupling between Mid-Infrared Localized Plasmons and Phonons

W. Wan

Xiaodong Yang
Missouri University of Science and Technology, yangxia@mst.edu

Jie Gao
Missouri University of Science and Technology, gaojie@mst.edu

Recommended Citation

W. Wan et al., "Strong Coupling between Mid-Infrared Localized Plasmons and Phonons," *Optics Express*, vol. 24, no. 11, pp. 12367-12374, Optical Society of America, May 2016.
The definitive version is available at https://doi.org/10.1364/OE.24.012367

Strong coupling between mid-infrared localized plasmons and phonons

Weiwei Wan,[1] Xiaodong Yang,[1,2] and Jie Gao[1,*]

[1]*Department of Mechanical and Aerospace Engineering, Missouri University of Science and Technology, Rolla, Missouri 65409, USA*
[2]*yangxia@mst.edu*
[*]*gaojie@mst.edu*

Abstract: We numerically and experimentally demonstrate strong coupling between the mid-infrared localized surface plasmon resonances supported by plasmonic metamaterials and the phonon vibrational resonances of polymethyl methacrylate (PMMA) molecules. The plasmonic resonances are tuned across the phonon resonance of PMMA molecules at 52 THz to observe the strong coupling, which manifests itself as an anti-crossing feature with two newly formed plasmon-phonon modes. It is also shown that the forbidden energy gap due to mode splitting is proportional to the overlapped optical power between the plasmonic resonance mode and the PMMA molecules, providing an effective approach for manipulating the coupling strength of light-matter interaction.

OCIS codes: (160.3918) Metamaterials; (250.5403) Plasmonics; (300.6340) Spectroscopy, infrared; (230.4555) Coupled resonators.

References and links

1. R. A. Shelby, D. R. Smith, and S. Schultz, "Experimental verification of a negative index of refraction," Science **292**(5514), 77–79 (2001).
2. J. Valentine, S. Zhang, T. Zentgraf, E. Ulin-Avila, D. A. Genov, G. Bartal, and X. Zhang, "Three-dimensional optical metamaterial with a negative refractive index," Nature **455**(7211), 376–379 (2008).
3. J. B. Pendry, "Negative refraction makes a perfect lens," Phys. Rev. Lett. **85**(18), 3966–3969 (2000).
4. X. Zhang and Z. Liu, "Superlenses to overcome the diffraction limit," Nat. Mater. **7**(6), 435–441 (2008).
5. J. B. Pendry, D. Schurig, and D. R. Smith, "Controlling electromagnetic fields," Science **312**(5781), 1780–1782 (2006).
6. X. Yang, J. Yao, J. Rho, X. Yin, and X. Zhang, "Experimental realization of three-dimensional indefinite cavities at the nanoscale with anomalous scaling laws," Nat. Photonics **6**(7), 450–454 (2012).
7. A. Alù, M. G. Silveirinha, A. Salandrino, and N. Engheta, "Epsilon-near-zero metamaterials and electromagnetic sources: Tailoring the radiation phase pattern," Phys. Rev. B **75**(15), 155410 (2007).
8. N. I. Landy, S. Sajuyigbe, J. J. Mock, D. R. Smith, and W. J. Padilla, "Perfect metamaterial absorber," Phys. Rev. Lett. **100**(20), 207402 (2008).
9. F. Cheng, X. Yang, and J. Gao, "Enhancing intensity and refractive index sensing capability with infrared plasmonic perfect absorbers," Opt. Lett. **39**(11), 3185–3188 (2014).
10. J. Ye, F. Wen, H. Sobhani, J. B. Lassiter, P. V. Dorpe, P. Nordlander, and N. J. Halas, "Plasmonic nanoclusters: near field properties of the Fano resonance interrogated with SERS," Nano Lett. **12**(3), 1660–1667 (2012).
11. F. Neubrech, A. Pucci, T. W. Cornelius, S. Karim, A. García-Etxarri, and J. Aizpurua, "Resonant plasmonic and vibrational coupling in a tailored nanoantenna for infrared detection," Phys. Rev. Lett. **101**(15), 157403 (2008).
12. X. M. Goh, Y. Zheng, S. J. Tan, L. Zhang, K. Kumar, C. W. Qiu, and J. K. W. Yang, "Three-dimensional plasmonic stereoscopic prints in full colour," Nat. Commun. **5**, 5361 (2014).
13. N. Liu, M. Mesch, T. Weiss, M. Hentschel, and H. Giessen, "Infrared perfect absorber and its application as plasmonic sensor," Nano Lett. **10**(7), 2342–2348 (2010).
14. H. Wang, Y. Yang, and L. Wang, "Wavelength-tunable infrared metamaterial by tailoring magnetic resonance condition with VO2 phase transition," J. Appl. Phys. **116**(12), 123503 (2014).
15. B. Luk'yanchuk, N. I. Zheludev, S. A. Maier, N. J. Halas, P. Nordlander, H. Giessen, and C. T. Chong, "The Fano resonance in plasmonic nanostructures and metamaterials," Nat. Mater. **9**(9), 707–715 (2010).
16. N. Liu, L. Langguth, T. Weiss, J. Kästel, M. Fleischhauer, T. Pfau, and H. Giessen, "Plasmonic analogue of electromagnetically induced transparency at the Drude damping limit," Nat. Mater. **8**(9), 758–762 (2009).
17. R. Taubert, M. Hentschel, J. Kästel, and H. Giessen, "Classical analog of electromagnetically induced absorption in plasmonics," Nano Lett. **12**(3), 1367–1371 (2012).
18. Z. Ruan and S. Fan, "Superscattering of light from subwavelength nanostructures," Phys. Rev. Lett. **105**(1), 013901 (2010).

#261972 Received 29 Mar 2016; revised 22 May 2016; accepted 23 May 2016; published 27 May 2016

19. L. Verslegers, Z. Yu, Z. Ruan, P. B. Catrysse, and S. Fan, "From electromagnetically induced transparency to superscattering with a single structure: a coupled-mode theory for doubly resonant structures," Phys. Rev. Lett. **108**(8), 083902 (2012).
20. W. Wan, W. Zheng, Y. Chen, and Z. Liu, "From Fano-like interference to superscattering with a single metallic nanodisk," Nanoscale **6**(15), 9093–9102 (2014).
21. A. Salomon, R. J. Gordon, Y. Prior, T. Seideman, and M. Sukharev, "Strong coupling between molecular excited states and surface plasmon modes of a slit array in a thin metal film," Phys. Rev. Lett. **109**(7), 073002 (2012).
22. D. J. Shelton, I. Brener, J. C. Ginn, M. B. Sinclair, D. W. Peters, K. R. Coffey, and G. D. Boreman, "Strong coupling between nanoscale metamaterials and phonons," Nano Lett. **11**(5), 2104–2108 (2011).
23. X. Zhang, D. Wu, C. Sun, and X. Zhang, "Artificial phonon-plasmon polariton at the interface of piezoelectric metamaterials and semiconductors," Phys. Rev. B **76**(8), 085318 (2007).
24. J. P. Long and B. S. Simpkins, "Coherent Coupling between a Molecular Vibration and Fabry–Perot Optical Cavity to Give Hybridized States in the Strong Coupling Limit," ACS Photonics **2**(1), 130–136 (2015).
25. A. Benz, S. Campione, J. F. Klem, M. B. Sinclair, and I. Brener, "Control of strong light-matter coupling using the capacitance of metamaterial nanocavities," Nano Lett. **15**(3), 1959–1966 (2015).
26. B. Lahiri, S. G. McMeekin, R. M. De la Rue, and N. P. Johnson, "Enhanced Fano resonance of organic material films deposited on arrays of asymmetric split-ring resonators (A-SRRs)," Opt. Express **21**(8), 9343–9352 (2013).
27. F. Cheng, X. Yang, and J. Gao, "Ultrasensitive detection and characterization of molecules with infrared plasmonic metamaterials," Sci. Rep. **5**, 14327 (2015).
28. L. Novotny, "Strong coupling, energy splitting, and level crossings: A classical perspective," Am. J. Phys. **78**(11), 1199–1202 (2010).

1. Introduction

Metamaterials are artificially engineered structures designed to exhibit extraordinary optical properties that are not achievable in natural materials. Metamaterials have been used to realize many intriguing applications such as negative refraction [1,2], super-resolution imaging [3,4], invisibility cloaking [5], subwavelength indefinite cavity [6], near-zero permittivity [7], and perfect absorber [8,9]. In particular, plasmonic metamaterials supporting localized surface plasmon resonances (LSPRs) can confine the electromagnetic fields at the subwavelength scale and therefore greatly enhance the near-field coupling effects and the light-matter interactions. Such capability of plasmonic metamaterials enables many biosensing applications such as surface-enhanced Raman scattering (SERS) [10] and surface-enhanced infrared absorption (SEIRA) [11].

In addition, plasmonic resonances can be simply tuned by varying the geometrical factors to exactly match the targeted optical frequencies from the visible [12] to infrared regime [13,14]. The interactions between different types of plasmonic resonances have resulted in extraordinary phenomena, such as Fano resonance [15], electromagnetically induced transparency [16], electromagnetically induced absorption [17], and superscattering behavior [18–20]. On the other hand, the coupling between plasmonic resonances and phonon vibrational resonances of molecules through near field interactions can give rise to a new set of splitting plasmon-phonon modes with anti-crossing behavior [21–23]. Such strong coupling can also be realized by using the Fabry-Pérot cavity [24]. The strong coupling can be controlled using the capacitance of metamaterial nanocavities [25]. Here, we explore the strong coupling between the mid-infrared localized plasmonic resonances in metamaterials and the phonon vibrational resonances of PMMA molecules, and demonstrate the anti-crossing feature with two plasmon-phonon eigenmodes. Furthermore, it is shown that the mode coupling strength can be controlled by the variation of the thickness of PMMA layer.

2. Strong coupling between plasmonic metamaterials and PMMA molecules

Figure 1(a) illustrates the schematic of plasmonic metamaterials used to study their interaction with PMMA molecules. A 50-nm-thick continuous gold film was deposited on a glass substrate with electron-beam evaporation. Then the designed cross-shaped aperture array was milled into the gold film using a focused ion beam (with the voltage and current of the ion beam as 30 kV and 100 pA), with the dimensions of aperture length $l = 0.8P$, and aperture width $w = 0.15P$, where P is the period of the cross-shaped aperture. Figure 1(b) shows a scanning electron microscope image of the top view of the fabricated plasmonic metamaterials. The optical properties of plasmonic metamaterials were simulated by a Finite Integration Time Domain solver (CST Microwave Studio software package). The permittivity

#261972 Received 29 Mar 2016; revised 22 May 2016; accepted 23 May 2016; published 27 May 2016

of gold in the infrared spectral regime is described by the Drude model $\varepsilon_{Au} = \varepsilon_\infty - \omega_p^2 / (\omega^2 + i\gamma_p \omega)$, where the background dielectric constant ε_∞ = 1, the plasma frequency $\omega_p = 1.37 \times 10^{16}$ *rad/s*, and the damping constant $\gamma_p = 4.08 \times 10^{13}$ *rad/s*. Due to the surface scattering, grain boundary effects, and the gallium ion contamination in thin films, the damping constant of the gold film is set to be five times as that of bulk gold in the simulation in order to match the experimental results. The optical reflection spectra were measured with a Fourier transform infrared spectrometer (FTIR, Nicolet 6700) connected to an infrared microscope. The normal incident light is polarized in *x* direction by using a linear polarizer. Figures 1(c) and 1(d) show the simulated and measured reflectance spectra of bare aperture arrays with different periods, respectively. The simulation and experimental results match well with each other. It is shown that the plasmonic resonance frequencies of cross-shaped apertures can be tuned in a broad band by stretching the period to cover the phonon vibrational frequency of PMMA molecules at 52THz.

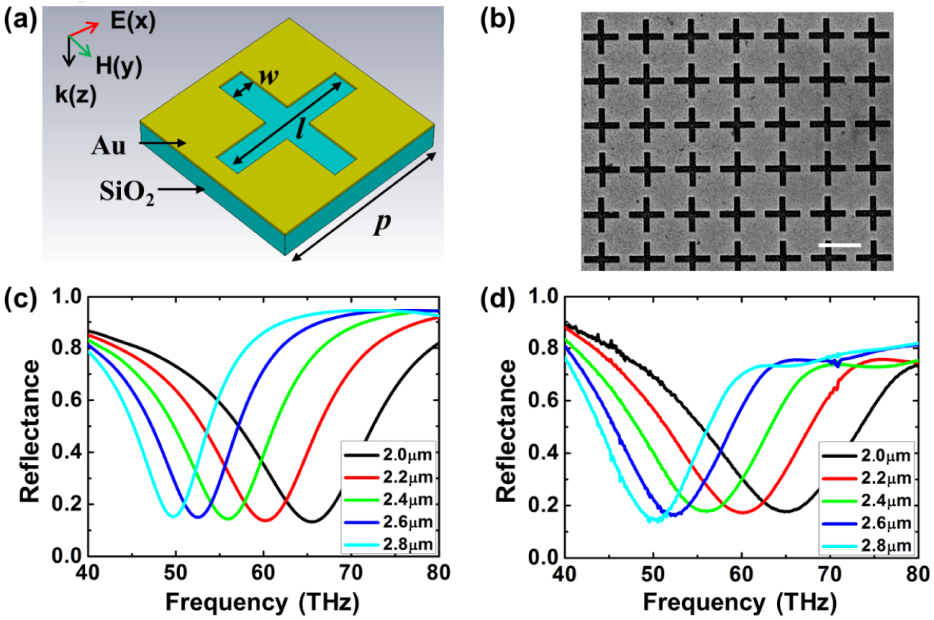

Fig. 1. (a) Schematic of one unit cell of the cross-shaped aperture array and the incident light polarization configuration. (b) A SEM image of the fabricated aperture array (Top View, scale bar, 2 μm). (c) Simulated reflectance spectra and (d) FTIR measured reflectance spectra of the bare aperture arrays with different periods *p*.

The top panel in Fig. 2 shows that the plasmonic resonance frequency of the bare aperture array with the period of 2.35 μm is ω_{bare} = 57 THz. In order to study the strong interaction between plasmon and phonon resonances, a thin layer of PMMA molecules dissolved in anisole (950A-2, Microchem) is deposited by spin coating on the top of the fabricated bare metamaterials. The PMMA film will introduce not only the phonon vibrational resonance but also the increased effective refractive index. The middle panel shows that the plasmonic resonance frequency is red shifted to ω_m = 52 THz for the uncoupled metamaterials coated with a 180-nm-thick PMMA film but in absence of the phonon vibrational resonance, where the permittivity of PMMA is assumed to be a constant (ε_{PMMA} = 2.2) without taking into account the phonon mode. The uncoupled plasmonic resonance frequency ω_m is designed around 52 THz in order to match the phonon vibrational frequency of PMMA molecules. The bottom panel in Fig. 2 shows the agreement between the simulated and FTIR measured reflectance spectra when considering the phonon vibrational mode in the permittivity of PMMA. The permittivity of actual PMMA film can be modeled as a Lorentz oscillator

#261972 Received 29 Mar 2016; revised 22 May 2016; accepted 23 May 2016; published 27 May 2016

by $\varepsilon_{PMMA} = \varepsilon_b - \varepsilon_{Lorentz}\omega_0^2/(\omega^2 + i\delta_0\omega - \omega_0^2)$, where the background relative permittivity of PMMA is ε_b = 2.2, and the Lorentz resonance frequency is ω_0 = 3.269 × 10^{14} rad/s (52 THz) [26,27]. The Lorentz permittivity $\varepsilon_{Lorentz}$ of 0.018 and the Lorentz damping rate δ_0 of 8.0 × 10^{11} rad/s have been selected to provide a close matching with the experimental result. The uncoupled plasmonic resonance (ω_m) strongly interacts with the phonon vibrational resonance of PMMA molecules (ω_0) in the near field, resulting in two coupled plasmon-phonon modes ($\omega_\pm$) that produce a unique dual resonance feature in the reflectance spectrum. The strong coupling between the localized plasmons and the phonons opens a reflectance window with two new reflectance minima around the frequency of 52 THz. The forbidden energy gap (Ω = ω_+ - ω_-) between the two coupled plasmon-phonon modes is found to be 2.6 THz.

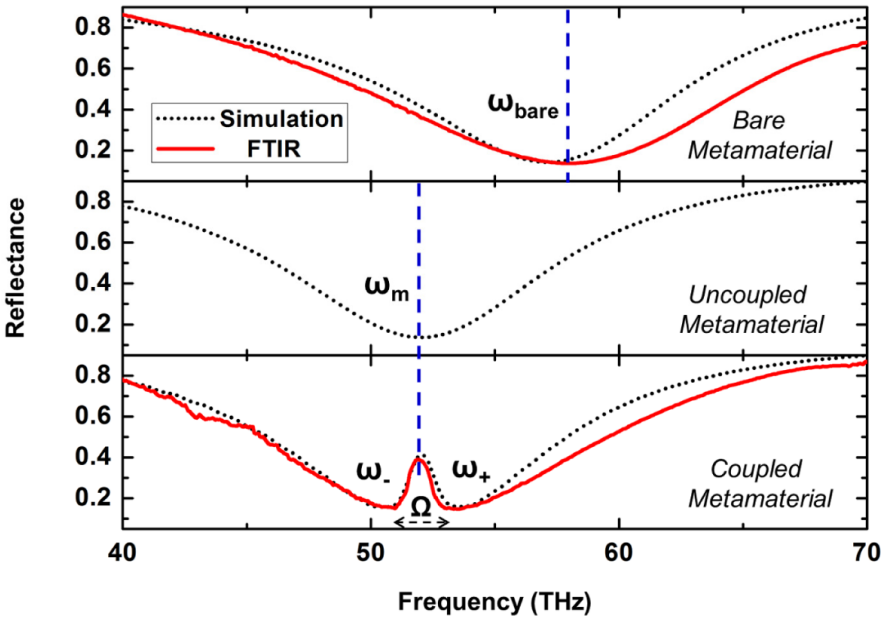

Fig. 2. Mode splitting induced by the strong coupling between the uncoupled plasmonic resonance and the phonon vibrational resonance of PMMA molecules. The black dotted curves and red solid curves represent the simulated and FTIR measured results, respectively. The period of aperture array is 2.35 μm. Top panel shows the plasmonic resonance of the bare metamaterial without PMMA. Middle panel shows the plasmonic resonance of the uncoupled metamaterial with 180-nm-thick PMMA coated on the top but in the absence of the phonon mode. Bottom panel shows two coupled plasmon-phonon modes the coupled system consisting of both the metamaterial and actual PMMA.

In order to demonstrate the expected anti-crossing behavior for strong coupling, twenty-four cross-shaped aperture arrays with different periods changing from 1.9 to 2.8 μm were fabricated and characterized. The geometrically stretching the dimensions of plasmonic metamaterials allows a stepwise sweep of the uncoupled resonance frequency ω_m across the phonon vibrational frequency of PMMA molecules. Figure 3(a) shows the reflectance spectra of bare metamaterials as a function of the resonance frequency of bare metamaterial ω_{bare}. Figures 3(b) and 3(c) show the good agreement between the simulated and measured reflectance spectra for the coupled systems as a function of the resonance frequency of bare metamaterial ω_{bare}, where the cross-shaped aperture arrays are coated with 180-nm-thick PMMA film on the top. The white dashed curves indicate the locations of reflectance minima. Due to the strong coupling between the plasmonic resonances and the phonon modes of PMMA molecules, we observe a clear anti-crossing behavior of two plasmon-phonon eigenmode branches, resulting in a forbidden energy gap.

#261972 Received 29 Mar 2016; revised 22 May 2016; accepted 23 May 2016; published 27 May 2016

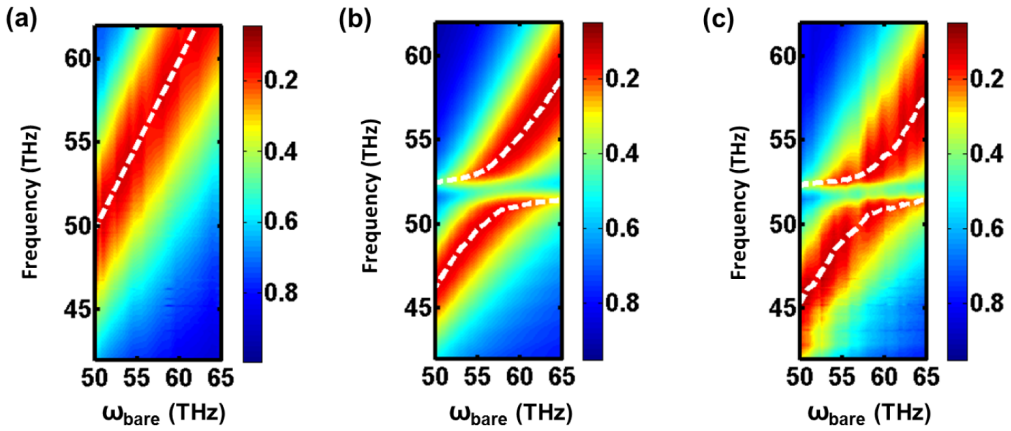

Fig. 3. (a) FTIR measured reflectance spectra of bare metamaterials as a function of the resonance frequency of bare metamaterial. (b) Calculated reflectance spectra for the coupled system. (c) FTIR measured reflectancee spectra for the coupled system. The white dashed curves indicate the reflectance minima.

3. Tuning the forbidden energy gap by varying the thickness of PMMA layer

The coupling strength between the plasmonic resonances and the phonon vibrational modes can be further tuned by the thicknesses of PMMA film. Here PMMA films with three different thicknesses of t = 40, 100, and 180 nm are spin coated on the cross-shaped aperture arrays with various periods. The thickness of PMMA film is controlled by varying the PMMA molecule concentration in anisole solvent and the spin-coating speed. The X-ray reflectivity measurement is used to measure the PMMA thickness of 40 and 100 nm, while the 180 nm thickness is measured by the cross-section characterization using a focused ion beam system. All the uncoupled plasmonic resonances are designed nearly equal to the phonon vibrational frequency of PMMA molecules at 52 THz. As shown in Fig. 4(a), the dual resonance features are found for all the three cases in both the simulated and measured reflectance spectra, and the resonances get stronger as the PMMA thickness is increased. The window reflectance maximum is about 25% for the thinnest PMMA layer of t = 40 nm, and it increases to 40% when t = 180 nm, indicating that the thicker PMMA layer will induce the stronger plasmon-phonon coupling strength. The change of coupling strength can also be revealed by the forbidden energy gaps between two plasmon-phonon eigenmode branches. As shown in Fig. 4(b), the forbidden energy gap Ω gets larger from 1.9 THz to 2.2 and 2.6 THz as the PMMA thickness is increased from 40 nm to 100 and 180 nm. These results match the analysis from the model of coupled harmonic oscillators, where the mode splitting gap increases with the coupling strength [22, 28]. As a result, the plasmon-phonon coupling strength can be controlled by varying the PMMA thickness. It is worth mentioning that, theoretically, the reflectance at the gap center (such as in Fig. 4(a)) could reach to 1 if the coupling strength between the plasmonic modes and the PMMA phonons is strong enough and both the optical loss of plasmonic modes and the damping loss of phonon vibrational modes in PMMA molecules can be neglected. However, in reality, there is non-negligible loss in the coupled system so that the reflectance peak within the forbidden energy gap will be lower than 1.

#261972 Received 29 Mar 2016; revised 22 May 2016; accepted 23 May 2016; published 27 May 2016

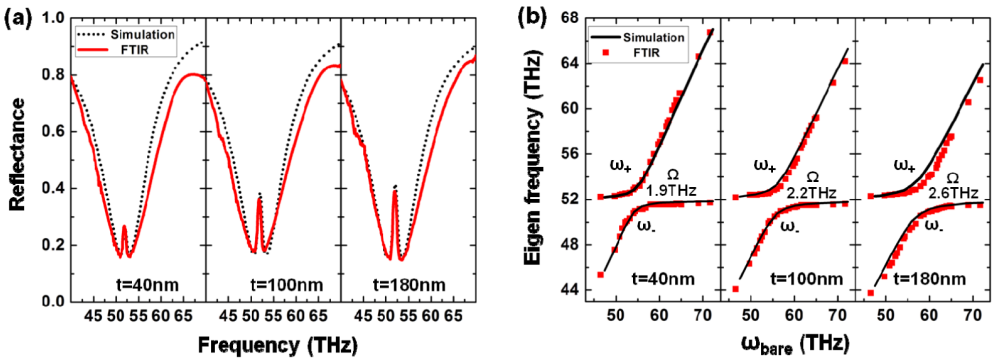

Fig. 4. (a) Simulated and FTIR measured reflectance spectra of the coupled systems with metamaterials coated with PMMA films of different thicknesses (40, 100 and 180 nm). The uncoupled plasmonic resonances are designed at 52 THz. (b) Simulated and FTIR measured resonance frequencies $\omega_{\pm}$ with respected to the resonance frequency of bare metamaterial ω_{bare}.

Since the electric field of plasmonic resonance mode exponentially decays above the metamaterial surface, the PMMA films coated on the top of metamaterials with different thicknesses will have different overlapped volumes with the confined plasmonic modes. In order to quantitatively study the relation between the coupling strength and the PMMA thickness, the electric field distribution of the coupled system at the middle plane of the cross-shaped aperture is calculated, as shown in Fig. 5(a). As expected, the electric field is mostly confined around the metamaterial surface, and decays fast into the PMMA film or the glass substrate. Figure 5(b) shows the electric field profile on the white dashed curve indicated in Fig. 5(a). The regions of I, II, and III represent the areas of glass substrate, gold layer, and PMMA film, respectively. The 1/e decay length of the confined electric field is about 350 nm above the metamaterial surface. Thus, the overlapped volume between the plasmonic resonance mode and the PMMA molecules significantly increases with the PMMA thickness, as long as the PMMA thickness is less than the 1/e decay length of 350 nm. It can then be assumed that the confined electrical field exponentially decays with a rate of $\alpha = 2.9\ \mu m^{-1}$ away from the metamaterial-PMMA interface, and can be described by $E = E_0 e^{-\alpha z}$, where E_0 is the electric field at the metamaterial surface. The total overlapped optical power between the plasmonic resonance mode and the PMMA molecules on the electric field profile can then be described as:

$$P_{tot} \propto \int_0^z E_0^2 \exp(-2\alpha z) dz \propto A(1-\exp(-2\alpha z)) + A_0, \quad (1)$$

where A is a coefficient, and A_0 is the overlapped optical power for zero PMMA thickness. Note that actually A_0 indicates the overlapped optical power between the plasmonic resonance mode and the PMMA molecules filled inside the cross-shaped apertures, which is not zero. Since the coupling strength depends on both the plasmonic near field intensity and the overlapped mode volume with PMMA molecules, the amount of the overlapped optical power P_{tot} described in Eq. (1) is proportional to the forbidden energy gap Ω as a function of the PMMA thickness, which can be calculated as,

$$\Omega = B(1-\exp(-2\alpha z)) + B_0, \quad (2)$$

where B and B_0 are two fitting parameters in THz. We simulated the forbidden energy gap for the PMMA thickness from 50 nm to 700 nm, as shown in Fig. 5(c). The fitting result for Ω using Eq. (2) with B = 2.4 THz and B_0 = 1.35 THz (black dashed curve) shows a good agreement with the simulated results (black squares) and the measured data for three PMMA thicknesses (red triangles). Since surface plasmons are confined around the interface at the metallic layer and the PMMA dielectric layer, as shown in Fig. 5(a), the plasmonic field will

#261972 Received 29 Mar 2016; revised 22 May 2016; accepted 23 May 2016; published 27 May 2016

be concentrated at the metal-PMMA interface and it will decay quickly far from the interface as the PMMA thickness increases. Thus, the coupling between the plasmonic modes and the PMMA molecules will be strong near the interface and gets weaker far away from the interface. Based on our analysis in Fig. 5(c), the forbidden energy gap grows quickly as the PMMA thickness increases within the decay length of 350 nm. For PMMA molecules more than 350 nm above the interface, the coupling strength between the plasmonic modes and the PMMA phonons is actually very weak so that the forbidden energy gap will be saturated at around 3.75 THz, due to the near-field effect of the plasmon-phonon coupling. It is shown that the control of overlapped optical power with different PMMA thicknesses provides an effective approach to tune the plasmon-photon coupling strength.

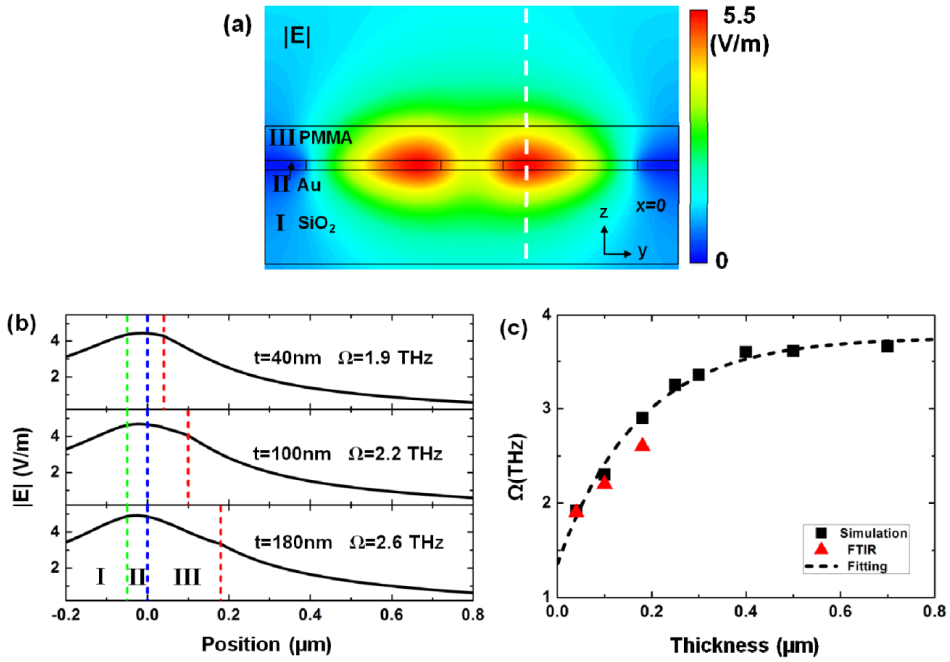

Fig. 5. (a) The cross-section electric field distribution of the coupled system at the phonon vibrational frequency of 52 THz. The normal incident electric field (1V/m) is *x*-polarized. (b) The electric field profiles on the white dashed curve in (a) for PMMA thicknesses of 40, 100, and 180 nm. The metamaterial surface (indicated by the blue dashed curve) is set at the z = 0 position. (c) The comparison of forbidden energy gap between the simulated, fitted, and FTIR measured results as the function of PMMA thickness. The fitting parameters in Eq. (2) are α = 2.9 μm^{-1}, B = 2.4 THz, B_0 = 1.35 THz.

4. Conclusion

We have demonstrated the strong coupling between the mid-infrared localized surface plasmon resonances in plasmonic metamaterials and the phonon vibrational resonances of PMMA molecules. The strong coupling presents as an anti-crossing feature with two newly formed plasmon-phonon eigenmodes. It is also demonstrated that the overlapped optical power between the plasmonic resonance mode and the PMMA molecules is a crucial parameter to determine the coupling strength for light-matter interaction and is proportional to the forbidden energy gap as the function of PMMA thickness. By changing the thickness of the coated PMMA film in the range of less than the decay length of the electric field, we can tune the forbidden energy gap. Our study provides an effective approach to manipulate the coupling strength for light-matter interaction by simply varying the overlapped volume between the optical resonance mode and the active medium. Our demonstration can also be used for mid-infrared molecular sensing applications.

#261972 Received 29 Mar 2016; revised 22 May 2016; accepted 23 May 2016; published 27 May 2016

Acknowledgments

The authors acknowledge support from the Office of Naval Research (ONR) under Grant N00014-16-1-2408, the National Science Foundation (NSF) under Grant DMR-1552871 and CBET-1402743, and U.S. Army Research Office Award No. W911NF-15-1-0477. The authors also acknowledge the facility support from the Materials Research Center at Missouri S&T.

#261972 Received 29 Mar 2016; revised 22 May 2016; accepted 23 May 2016; published 27 May 2016